EXPERIMENTAL DEFORMATION OF MULTILITHOLOGIC SPECIMENS SIMULATING SEDIMENTARY FACIES CHANGES

A Thesis

by

LAWRENCE DANA DYKE

Submitted to the Graduate College of
Texas A&M University
in partial fulfillment of the requirement for the degree of

MASTER OF SCIENCE

December 1976

Major Subject: Geology

EXPERIMENTAL DEFORMATION OF MULTILITHOLOGIC

SPECIMENS SIMULATING SEDIMENTARY FACIES CHANGES

A Thesis

by

LAWRENCE DANA DYKE

Approved as to style and content by:

(Chairman of Committee)

(Head of Department)

(Member)

(Member)

(Member)

December 1976

ABSTRACT

Experimental Deformation of Multilithologic Specimens Simulating Sedimentary Facies Changes. (December 1976)

Lawrence Dana Dyke, B.Sc., University of British Columbia

Chairman of Advisory Committee: Dr. J. M. Logan

Study of White Uplift in northern Yukon Territory, Canada, where fault-bounded structural relief is coincident with a carbonate to clastic facies change, has suggested that sedimentary facies changes are important in controlling the location of deformation. To investigate this problem, three-layered specimens of Coconino Sandstone (11 by 3 by 3 cm., 1 cm. layer thickness), each containing a block inclusion of Indiana Limestone, polycrystalline halite, modeling clay or Tennessee Sandstone in the middle layer, have been shortened, dry, at room temperature, confining pressures of 1.0, 2.0 or 3.0 kb. and at a shortening rate of 10^{-4}/sec. Deformation in the outer layers takes place immediately adjacent to the inclusion regardless of its location relative to the ends of the specimen, if the relative strength of the inclusion is less than that of Coconino Sandstone. Study of the microfracture abundance in the outer layers of specimens containing limestone inclusions indicates that the differential stress required for grain failure is reached first in small areas adjacent to the inclusion. These stress concentrations are caused by compressive bending stresses generated over parts of the limestone inclusion that expand perpendicular to the load direction. Shearing stresses operating between the inclusion and outer layers are responsible for the expansions.

The localized deformation is due to a contrast in scale-independent mechanical properties, suggesting a mechanism that may be operative at natural lateral lithologic contrasts.

ACKNOWLEDGMENTS

This study was made possible through the support of the faculty and staff and the facilities of the Center for Tectonophysics, Texas A&M University. I wish to thank my committee chairman, Dr. J. M. Logan, for his patience and scientific direction. Committee members, Drs. M. Friedman, D. A. Fahlquist and D. W. Stearns provided invaluable criticisms. J. Magouirk kept the experimental apparatus in working order.

Special thanks is due Dr. C. C. Mathewson for his interest, encouragement and, in the later stages, clerical support for the study. Karen McBride and M. F. Fahy provided encouragement, advice and their skills for the review of the manuscript.

Finally, I must thank my friend Dr. D. K. Norris of the Geological Survey of Canada, for the opportunity to do the field work which led to the discovery of the problem.

The research was supported by National Science Foundation Grant GA-36127X.

TABLE OF CONTENTS

LIST OF FIGURES

LIST OF PLATES

INTRODUCTION

Origin of the Problem

At White Uplift, one of several uplifts in the northern Canadian cordillera, structural relief of up to 3,600 meters occurs over an area of only 100 square kilometers (Norris, D. K., 1973; Dyke, 1972). This deformation is coincident with a carbonate accumulation that grades laterally into clastic rocks in sections close-by (Lenz, 1972; Norris, D. K., 1973). Because no evidence for a vertical maximum compressive stress can be found, it is here hypothesized that the deformation is the result of a horizontal maximum compressive stress and has been localized by the original sedimentary rock contrast.

Sedimentary facies change, where one rock type is replaced laterally by another, are an integral part of many sedimentary sequences. A contrast in mechanical behavior across a facies boundary might produce, under a given loading condition, a corresponding lateral contrast in the intensity and style of deformation. This study is an experimental investigation to determine if and why lateral lithologic variations influence the position as well as the type of deformation.

The problem is approached by experimentally deforming a simplified model of a facies change. These experiments use real rocks compressed under confining pressures to 3.0 kilobars, dry, at room temperature and at a shortening rate of 10^{-4}/second. In these models it is the mechanisms that localize deformation that are sought rather than the genera-

---

The citations on the following pages follow the style of the Bulletin of the American Association of Petroleum Geologists.

tion of a scale model of an uplift. Scale-independent mechanical properties by which deformation is localized offer a means for predicting how field occurrences of similar contrasts may behave. The results of these experiments suggest that effects of lateral lithologic changes should be anticipated in field structural analyses and that they may exert a significant influence on the total deformation picture in any deformed sedimentary sequence. At the same time, no attempt (save for the consideration of White Uplift) has been made to test the applicability of the experimental conclusions with field observations.

Concept of a lateral lithologic change capable of controlling deformation

In nature, facies boundaries are commonly subtle changes governed by the sedimentary environment. Most often, a gradual tapering or pinching-out of a lithology, or transition from one lithology to another within an interval of roughly constant thickness, is involved. Transgressive-regressive cycles in clastic basins characteristically result in lenses and tongues of sand enclosed in shales (Figure 1a). A transition-type facies change is often produced by the gradual increase in shale content basinward from a carbonate shelf (Figure 1b). For the purpose of this study, modelling a facies change involves a geometrical simplification. Such a simplification is difficult to reconcile with a transitional-type change. However, the case of a rapid transition may be approximated by a boundary perpendicular to layering.

Abrupt facies changes are not altogether rare in nature. Gradations from carbonates to shale over distances of from one mile to a

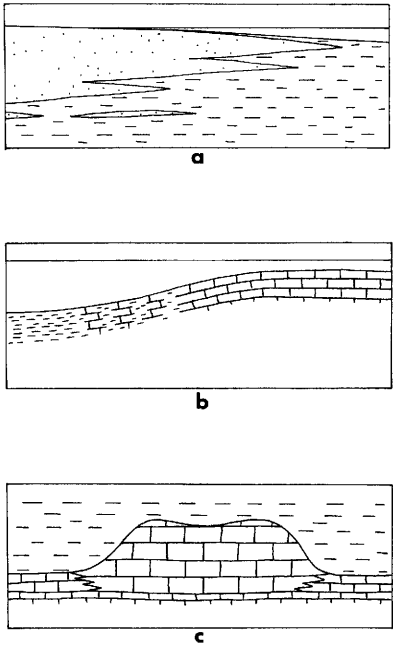

Figure 1. Generalized hypothetical facies changes. a. Clastic basin transgressive-regressive intertonguing; b. carbonate shelf-shale basin transition; c. carbonate reef enclosed in shales.

few tens of feet may be seen in the Middle Devonian shelf-basin transition in the northern Canadian cordillera (Noble and Ferguson, 1973). Cook (1970) has shown a long-supposed fault to in fact be a facies boundary. At his locality in the southern Canadian cordillera, Middle and Upper Cambrian, dominantly carbonate facies of the eastern Main Ranges grade, over a distance of less than half a mile, into slates of the western Main Ranges. Moreover, he has noted an apparent localization of deformation about the facies change, the style of the deformation being unique within his study area. A belt of tight, disharmonious folds coincides closely with the facies change in the southern part of his area and a broader belt of folds and thrust faults follows the change in the northern part. In the relatively undeformed terrain of the western Canadian platform, Blanchet (1957) has noted an increase of fracture density with increasing proximity to a carbonate reef. Reefs are commonly seen to be enclosed in shales on the platform and as such are good examples of a lithology of restricted lateral extent (Figure 1c). The transition from dolomitized to non-dolomitized carbonates may also provide a very abrupt lithologic transition. As a final example, the formation of barrier islands involves sand deposition with fringing mud deposition, i.e., a sandstone body of restricted lateral extent enclosed in shales. Just such a configuration is seen in the Tertiary of southern California where turbidite lenses decrease from a thickness of 1,000 feet to nothing in lateral distances of less than one mile (W. Doyle, pers. comm., 1975).

DESIGN OF THE SPECIMEN

Specimen configuration

The design of the model or specimen requires fitting what is known about the geology to the constraints of the experimental method. In this study the model must incorporate two aspects of a facies change assumed to be important: lithology and geometry. However, even these aspects must be idealized due to limitations imposed by specimen preparation techniques. If the model does show localized deformation and it is desired to evaluate its geological significance, then a hypothesis based on the behavior of the model must be developed to explain the localization of the deformation. If such a hypothesis is based on those characteristics of the specimen that exist in nature, then grounds for a correlation with nature may exist.

In simple terms, the original geometry of any facies change will lie between two end-members. At one extreme is no facies change, i.e. a simple layered package in which all lithologies remain at constant thickness with indefinite lateral extent. The other extreme is an abrupt boundary, perpendicular to layering, between two lithologies comprising the same layer. Between these two extremes any manner of change from one lithology to another may be imagined, from a sharp planar boundary inclined at any angle to the layering to a gradual transition zone separating the two facies. Any localization of deformation due to a lateral lithologic change would be expected to become less restricted as the abruptness (angle or rate of transition) of the change is decreased.

A lateral rock contrast simulating a facies change may be incorpo-

rated in a specimen made of three layers: one layer containing the contrast and two others which are continuous above and below (Figure 2). Choosing the shape of the contrast depends on three factors. First, specimen preparation techniques limit the choice of lithologic contacts to planar surfaces. Second, the mechanical properties of a planar facies boundary must be considered. The tapering model, depending on orientation, could offer a very favorable predetermined surface for shear displacement (Figure 2a). While this mechanism may operate at a natural counterpart, in a specimen it would probably tend to dominate at least the early stages of deformation and would not necessarily be the result of a mechanical contrast. Only orientations parallel and perpendicular to layering are suitable in terms of not containing shear components resolved from a load parallel to layering. Third, the lateral extent of facies to be considered must be decided. The two lithologies of a single facies change can extend away from the boundary almost indefinitely (Figure 2b) or one lithology can be of very restricted lateral extent (Figure 2c).

If a single facies change is simulated (Figure 2b), either lithologic segment would hardly be longer than that representing a restricted facies as in Figure 2c. Therefore a single-facies-change specimen might tend to act as a restricted-facies specimen, the only difference being that the lithology representing the restricted facies is moved to one end of the specimen.

To minimize the importance of undesirable effects of the loading condition in a rock deformation apparatus, a facies change of restricted lateral extent is chosen (Figure 3). This enables the lateral lithologic contacts to be kept away from the ends of the specimen where a frictional

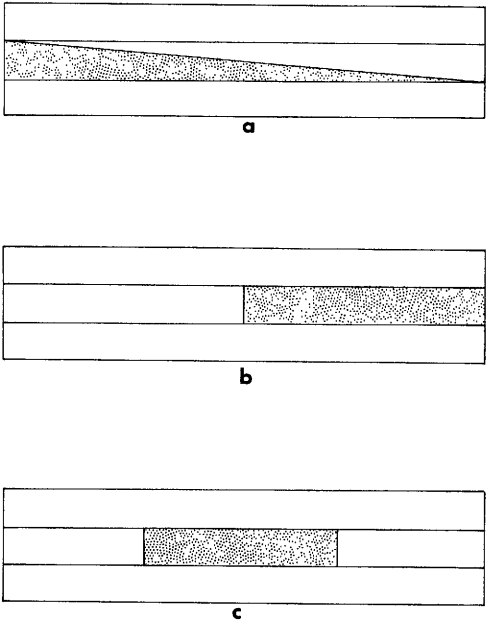

Figure 2. Simplified models of generalized facies. a. Wedge of contrasting lithology representing one tongue in a natural counterpart; b. distinct boundary representing rapid carbonate to shale transition; c. enclosed contrasting block representing a facies of restricted lateral extent.

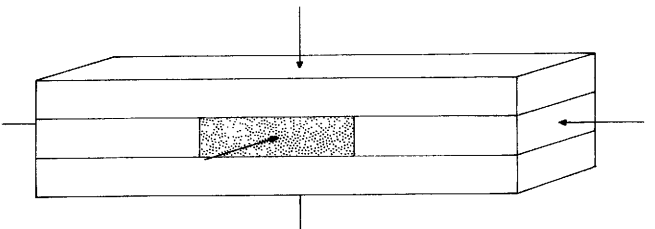

Figure 3. Basic specimen configuration. Stipled portion represents the block inclusion. Arrows parallel to the long axis represent the direction of the applied load. Other arrows represent the confining pressure. Figure approximates actual size of specimen.

restraint is offered against the loading pistons. To simplify the stress field within the specimen the length to width ratio of the specimen (aspect ratio) is made small enough to avoid any tendency toward folding. To prohibit folding, the aspect ratio of a beam cannot exceed about 4:1 for most rock materials (as a very crude guideline, it was assumed for the purpose of design that the presence of the inclusion would have no influence on overall stability). While individual layers of the specimen have aspect ratios of 10:1 to 12:1, the support offered by the rest of the specimen for each layer should act to oppose folding. Furthermore, Handin, et al.(1972) have shown that beams of a certain sandstone (Coconino Sandstone) having aspect ratios of up to 13:1 are not likely to fold. The use of such a material should ensure that folding does not take place.

Specimen dimensions

The limiting factor on overall dimensions is the piston diameter of the triaxial apparatus (Handin, et al., 1972). An approximately square cross-sectioned specimen with an aspect ratio of four allows a length of approximately 13 cm. The layers are of equal thickness with the central layer divided into three approximately equal portions. The central block is referred to as the inclusion and is composed of contrasting rock types as described below.

In practice, dimensions range as follows:

Overall length:	13.2 ± 0.5 cm.
Overall width:	2.8 ± 0.3 cm.
Overall depth:	3.3 ± 0.3 cm.
Individual layer thickness:	1.1 ± 0.1 cm.

Length of central layer segments: 4.5 ± 0.5 cm.

The average area perpendicular to the load direction is 10.17 cm^2 with a standard deviation of 0.36 $cm.^2$ Having the layers of equal thickness allows an equal influence of inclusion behavior on each outer layer. Resulting permanent deformation in each outer layer, if simultaneous, should be due to the same mechanism because of the symmetry of the specimen.

Specimen lithologies

The selection of lithologies is based on a tentative hypothesis that deformation is localized because of a contrast in bulk mechanical behavior between the inclusion and the surrounding material. Rock types are chosen to provide contrasts in terms of Poisson's ratio and relative strength. If a lithology having a high Poisson's ratio is enclosed in a material of lower Poisson's ratio, a tendency toward differential expansion perpendicular to the load direction would occur along the middle layer. This was initially considered the mechanism that would localize deformation and different lithologies for the inclusion were chosen so that the intensity of this effect could be varied.

No rigorous attempt was made to employ lithologies exactly matching those of natural counterparts. While this statement seems in contradiction to one of the basic assumptions defining the problem, it must be remembered that the problem itself is to find a mechanism related to deformational properties of rocks. Therefore material of well known mechanical properties should be most conducive to this goal. Limestone has almost invariably been found to have a higher Poisson's ratio than sandstone (Handin, 1966; Obert and Duvall, 1967). While shale should be

considered since it is a common component of facies changes, its granular deformation mechanisms are largely unknown, making it less useful than a material that lends itself to microscopic petrofabric analysis. Microfracturing of quartz grains and twinning of calcite have been shown to be reliable indicators of principal stress orientations and deformation intensity (Friedman, 1963), quantities that are desirable in determining if deformation may be localized.

Description of lithologies

The four lithologies used are Coconino Sandstone, Indiana Limestone, polycrystalline halite and Tennessee Sandstone. They have been employed extensively in geologically oriented experimental rock deformation studies and were chosen on the basis of their known deformational behavior (Handin et al., 1972; Min, 1975). However, the descriptions given are for specific quarry shipments as the materials can vary in mechanical properties from lot to lot.

Coconino Sandstone (Permian, Arizona) is used for the enclosing material in all specimens. It is fine to medium-grained with the grains mostly of subrounded to subangular quartz and cemented with clay that forms fine partings and occasionally coarser clots between grains. A few grains contain relic, healed microfractures having a stipled appearance. In thin section, alternating laminae of fine and medium grains are often seen. There was no noticeable control of microfracture distribution associated with changes in position of laminae in deformed specimens. This sandstone has a transition from brittle to macroscopically ductile deformation at about 2.0 kb., room temperature and a shortening rate of 10^{-4}/second. Increasing the confining pressure to 3.0 kb. per-

mits investigation of the complete brittle-ductile range of behavior.

Indiana Limestone (Mississippian, Indiana) is the lithology most frequently used for the inclusion. It consists of poorly sorted organic clasts commonly replaced by coarse sparry calcite in a micritic to finely sparry matrix. Both the Coconino and Indiana have approximately the same porosity (10 - 15%). Under the test conditions, this limestone has a brittle-ductile transition at approximately 0.2 kilobars confining pressure.

Comparing the two for their mechanical properties, Handin et al. (1972) show that Indiana limestone reaches its yield point at axial shortenings far smaller than those required for macroscopic fracture or cataclasis in Coconino Sandstone at the same confining pressure. Thus, while the sandstone is still behaving elastically with a relatively small Poisson's ratio, the limestone is undergoing permanent deformation. As the limestone enters the ductile mode, its Poisson's ratio will increase because of the onset of calcite twin gliding. Pore collapse tends to offset this effect at first but probably becomes less important as shortening proceeds.

Polycrystalline halite, manufactured by casting sodium chloride for cow licks, is used as the inclusion that most quickly approaches a Poisson's ratio of 0.5 during post-yielding deformation (Serata et al., 1972). Its brittle-ductile transition occurs at a confining pressure of less than 0.1 kb.

Tennessee Sandstone (Pennsylvanian, Tennessee) is used for a few of the inclusions to provide an inclusion that is stronger than the enclosing Coconino Sandstone. Tennessee Sandstone is a very well sorted, fine-grained, virtually pure quartz sandstone with a porosity estimated

to be less than 10%. It remains brittle throughout the range of confining pressures used. Finally, modelling clay is used in a few experiments to approximate an incompressible substance having no shear strength. The purpose is to simulate having the confining pressure acting in the space occupied by the inclusion. This will test the influence of the specimen geometry on the style of deformation.

EXPERIMENTAL PROCEDURE

Specimen preparation

All materials are rough-cut on a diamond saw and finished into the various layers with orthogonal sets of parallel faces on a surface grinder. The polycrystalline halite is hastily cut with water coolant and any pitted zone removed by the grinding procedure. The most difficult stages are assuring: (1) perpendicularity of the specimen ends and laterally touching surfaces to the center line of the specimen; and (2) equality of length of the three layers. Layer or layer segments ends could be ground to a tolerable degree of orthogonality by gripping the specimen or portions of it in a lathe chuck. Layer-lengths are kept equal to a tolerance of 0.0025 cm. using a vernier calipers. All dimensions of each specimen were recorded.

Smoothness of layer-surfaces is indicated in microscopic examination of thin sections. At 100x magnification, the truncated edges of quartz and calcite grains appear as essentually flat surfaces. The major contributor to the surface roughness would be any irregular spaces between grains, usually amounting to only a small fraction of a grain diameter.

Apparatus

The rock deformation apparatus consists of a screw-driven press that axially loads a specimen confined in an oil-filled pressure vessel. A detailed description of the apparatus is given in Handin et al. (1972). During the tests, force and displacement are plotted on an X-Y recorder from electrical output supplied by a force-gauge and external transducer,

respectively. Confining pressure is monitored with a hydraulic pressure gauge. The accuracies of the force displacement and confining pressure measurements are of the order of 1.5 percent.

Experimental procedure

Preparatory to insertion in the apparatus, each specimen is stamped with a one-tenth inch inked grid on the side exposing the inclusion. After the ends of each specimen are lubricated with Molykote (a commercially prepared mixture of grease and finely divided molybdenum disulphide) they are jacketed with two layers of polyolefin shrink-tubing. A lead shield is placed between the two jackets and over the inclusion to prevent intrusion of the jacketing into a hole where the corners of the inclusion may have broken.

All experiments are run as compression tests, dry, at room temperature and a shortening rate of 10^{-4}/second. Only confining pressure and axial shortening are varied.

Confining pressures: Three confining pressures, 1.0, 2.0 and 3.0 kb., are used. These values allow brittle, transitional and macroscopically ductile behavior, respectively, for the Coconino Sandstone at the experimental conditions used. They also include a range of confining pressures that would be expected in many sedimentary basins.

Axial Shortening: Tests are run to one of three degrees of shortening so that the development of deformation can be observed. These degrees are defined with respect to the shape of the force-displacement plot for each specimen. Each curve's character is derived mainly from the behavior of the Coconino Sandstone because this sandstone's failure

or yield strength is considerably greater than that of either the limestone or halite. The fracture or yield point expressed on a particular plot is used as the main reference for stopping tests.

An incipient failure or stage 1 test (Figure 4) is performed by stopping the test just as the force-displacement plot begins to decrease rapidly in slope. From experience gained with specimens shortened to failure, this decrease signifies that failure (ie. a sudden drop in differential load) is imminent. For both a fracture and a yield condition, the appearance at stage 1 is almost the same (Figure 5). The intent of this test is to observe the position and intensity of any zones of early intragranular deformation.

Failure or stage 2 tests are produced at 1.0 kb. confining pressure when the displacement is stopped immediately upon the first sudden and audible force drop (Figures 4, 5a, 6). At the higher confining pressures, this becomes a yield test and is the result of stopping displacement as soon as the rapid change in slope of the plot has ceased. A distinct yield point is produced at 2.0 kb. (Figures 4, 5c, 5d) but work hardening obscures this at 3.0 kb. (Figure 6).

Post-failure, post-yield or stage 3 tests are those for which displacement is carried considerably beyond the initial failure or yield point, usually to an overall shortening of about 3% (Figure 4). Inspection of the force-displacement plots for these experiments run at 2.0 kilobars show a well defined yield point with little or no force drop but usually a slight increase as shortening continued (Figure 5c, 5d).

A few specimens were tested twice, once to stage 2 and again to stage 3, allowing examination of how initial fractures may have influ-

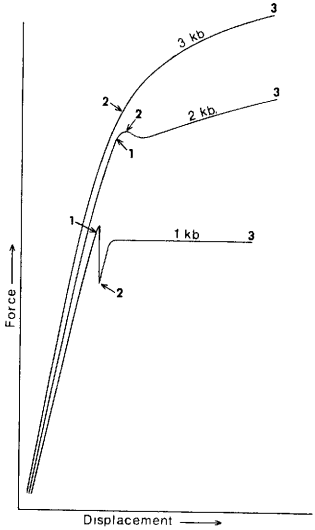

Figure 4. Idealized force-displacement curves showing the stages (1, 2, 3) of shortening referred to in the text. Curves are labeled according to confining pressure.

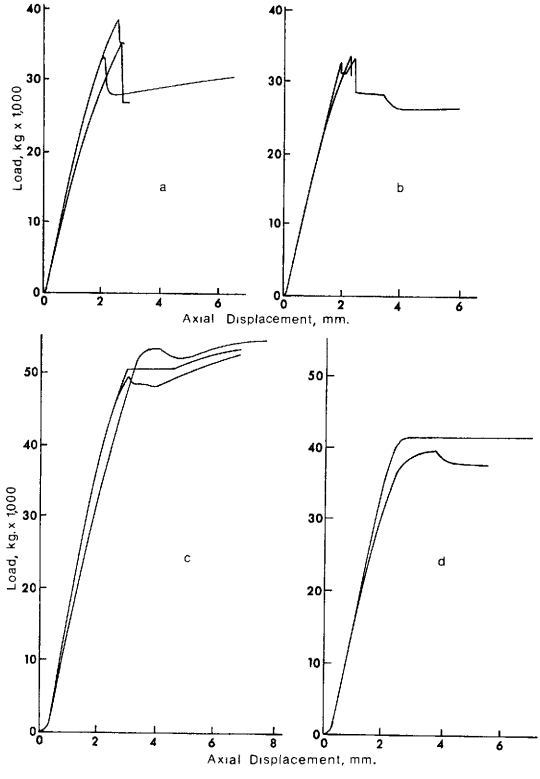

Figure 5. Representative force-displacement curves for specimens. a. Limestone inclusion, 1.0 kb confining pressure; b. halite inclusion, 1.0 kb; c. limestone inclusion, 2.0 kb; d. halite inclusion, 2.0 kb.

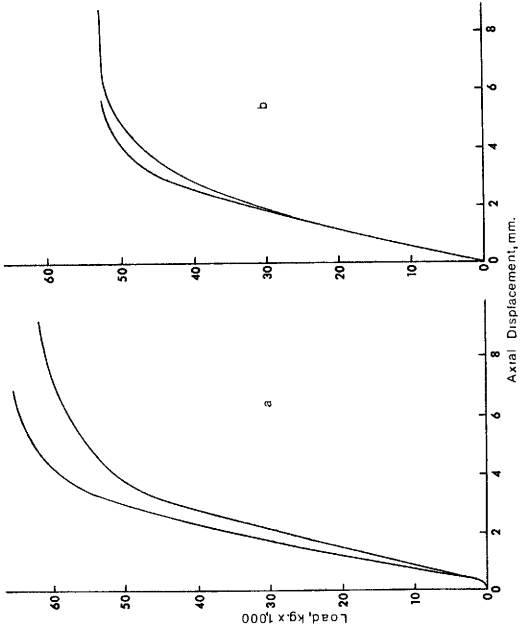

Figure 6. Representative force-displacement curves for specimens. a. Limestone inclusion, 3.0 kb; b. halite inclusion, 3.0 kb.

enced further deformation.

The various stages of shortening were employed so that development of deformation could be observed. Stage 1 tests allow observation of early-formed microfractures before they were partly obliterated by macroscopic failure. All tests allow observation of changes in position and intensity of micro- and macroscopic deformation.

Upon completion of a test, each specimen is unjacketed and preserved in a coating of epoxy cement. Slabs perpendicular to layering and parallel to the long axis are cut for thin sectioning. Because of the complex structure of the specimens, no attempt is made to reduce the force-displacement data to stress-strain data. Instead, loads at the failure or yield points are normalized to allow some comparison of these strengths between different types of specimen (Table 1).

Observations and measurements

Macroscopic deformation in the form of fractures, shear zones, localized shortening and changes in layer thickness was observed. Petrofabric and strain measurements were made on thin sections and in hand specimen to gain a more detailed understanding of deformation in the outer layers and inclusion.

Mapping of microfractures. The distribution of microfractures in grains of the Coconino sandstone is used to detect locations of high differential stress in the outer layers. Microfracture densities are mapped in thin section by making optical traverses at two millimeter intervals parallel to the ends of an outer layer. The number of microfractured grains crossed per two millimeters of traverse is counted and the number

Table 1

Data for Experimentally Deformed Specimens

Specimen	Confining Pressure, kb.	Degree of Shortening	Shortening to failure or yield point, %	Maximum Load, Normalized, Kg/cm^2
		Indiana Limestone inclusion		
1	1.0	Stage 1	2.2	3410
2	1.0	2	2.1	3750
3	1.0	2	1.9	3880
3 reloaded	1.0	3	4.0*	3070
4	1.0	2	2.1	3550
4 reloaded	1.0	3	4.5*	2970
5	1.0	3	4.3	3600
6	1.0	3	1.9	3870
7	2.0	2	2.7	4770
8	2.0	3	2.3	5080
9	2.0	3	2.4	4760
10	2.0	3	2.9	5490
11	3.0	2	2.7	5400
12	3.0	3	7.1*	6180
13	3.0	3	5.2*	6570
14	3.0	3	5.2*	5030
		Limestone inclusion lubricated		
15	1.0	2	2.2	3690
16	1.0	2	2.1	4120
17	1.0	2	2.3	4370
		Polycrystalline halite inclusion		
18	1.0	2	1.7	3310
19	1.0	3	1.5	3260
20	1.0	3	1.5	3130
21	1.0	3	1.5	2850
22	2.0	1	2.1	3580
23	2.0	3	2.1	4100
24	2.0	3	2.5	4020
25	3.0	2	4.1*	5300
26	3.0	3	5.3*	5350

Table 1 continued

Specimen	Confining Pressure, Kb.	Degree of Shortening	Shortening to failure or yield point, %	Maximum Load, Normalized, Kg/cm^2
		Clay inclusion		
27	1.0	2	1.3	2310
28	1.0	2	1.9	2990
		Tennessee Sandstone inclusion		
29	1.0	2	2.4	4890
30	2.0	2	3.5	7250
31	2.0	3	3.2	6180
		Three layers of Coconino Sandstone		
32	1.0	2	2.3	5190
33	1.0	2	2.3	5070

*Shortening at maximum piston displacement.

per millimeter plotted on a grid corresponding to the position on the specimen. These numbers could be contoured directly but to make the contours more representative of the overall distribution, a smoothing operation was performed. In the center of each square of the grid, the average of the four numbers occupying the corners is plotted. These averages are then contoured. By this method, very local anomalous concentrations are partially damped out. If every grain is fractured, the average grain size of the sandstone allows a maximum density of eight grains per millimeter. Microscopic feather fractures (Friedman and Logan, 1970) or the narrow zone of demolished grains along macroscopic shear zones are not included in the counts. They are the result of processes directly associated with movement along the macrofracture and as such are not indicators of the overall stress pattern.

A more precise method would be to count the total number of microfractures in each grain. This was done for comparison on one specimen and the only difference is that the microfracture concentrations are roughly twice as pronounced while the overall distribution pattern is the same. The former method is used for expediency.

Direct surface strain measurement. The stamped grid segments on limestone inclusions are measured with a binocular microscope, and strains are calculated in the direction of the axial load for specimens subjected to stage 3 shortening. Strains caused by lesser degrees of shortening are too small to be measured. Because of the indistinct nature of the grid lines under magnification, all linear measurements are repeated using two methods of calculating strain to check for reproducibility. Grid segments 5 mm. long were used, allowing about eight strain determina-

tions to be made across an inclusion. One method was simply to compare the lengths of the deformed segments with the undeformed length along a given direction. The other involved using the two sides and a diagonal of grid squares as if they were strain-gauge rosettes (Jaeger and Cook, 1969). Separate measurements were made for each method.

Internal strain measurements. The measurement of principal strain magnitudes within selected limestone inclusions was attempted using the calcite strain-gauge technique of Groshong (1972). Strain determinations in domains at the ends and in the middle of inclusions were attempted in an effort to compare the results to the corresponding surface-strain measurements. In addition, the calcite twin lamellae spacing index (average of number of lamellae per millimeter when viewed on edge in all twinned grains for a given domain) also was determined as a rough measure of deformation (Handin, et al., 1972, Figure 18).

EXPERIMENTAL RESULTS

Descriptions of deformation seen in hand specimen and in thin section are given for each successive confining pressure according to inclusion lithology. The most obvious and universal observation for specimens containing limestone or halite inclusions is the fact that permanent deformation (either macroscopic fracturing or cataclasis) of the enclosing material is confined to the area in each outer layer against or immediately adjacent to the inclusion. This occurs even when the inclusion is moved toward one end of the specimen (Plate 1). Microfracture distributions in the outer layers are mapped for all confining pressures and show a consistent pattern relative to the inclusion. No observable deformation due to compression occurs in the sandstone components of the middle layer when limestone or halite serves as the inclusion. Representative force-displacement curves are shown in Figures 5 and 6 and normalized loads at failure or yield points for all specimens are listed in Table 1.

Tests at 1.0 kb.

Limestone inclusion. In specimens loaded to stage 2, failure is always manifest by a single distinct shear fracture in each outer layer, one conjugate to the other and each inclined in a direction parallel to the long dimension of the specimen (Plate 2, see arrows). This pattern appears in each of the six specimens deformed under these conditions. Fractures terminating at inclusion corners are never developed. Instead, the fractures meet the inclusion at points distinctly inward from the corners (Plate 2, points a). It is noteworthy that these fractures show

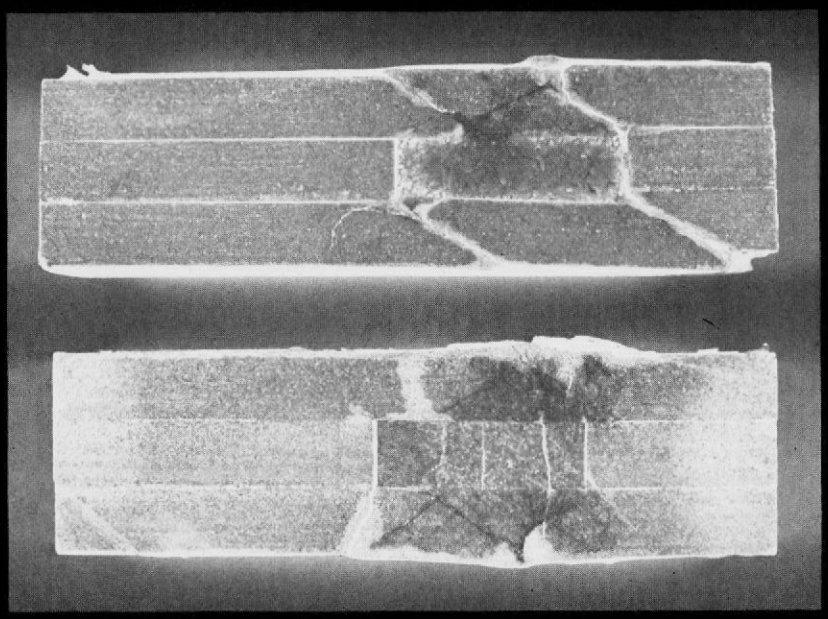

Plate 1. Stage 3 specimens containing halite (upper) and limestone (lower) inclusions, deformed at 1.0 kb.

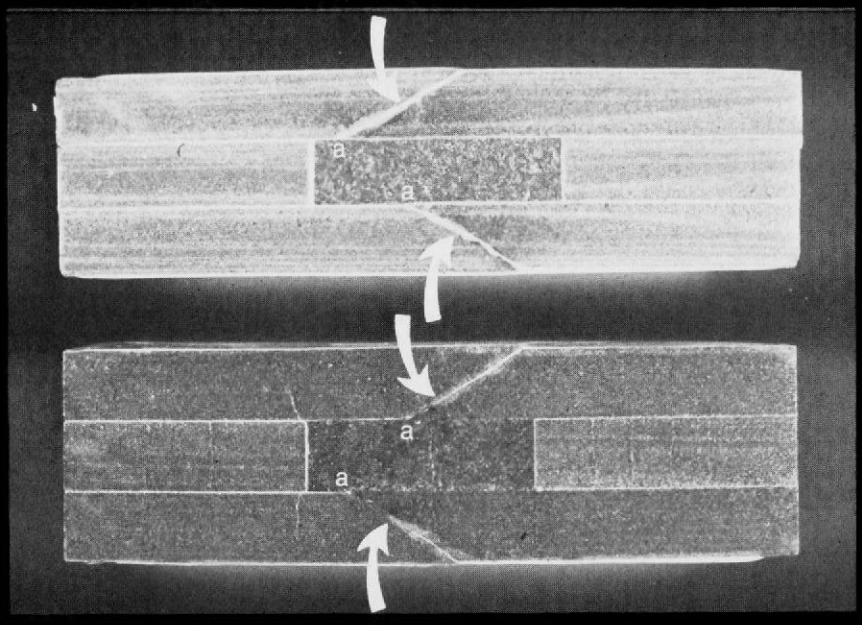

Plate 2. Stage 2 specimens containing limestone inclusions deformed at 1.0 kb. Arrows point to initial fractures.

no continuation within the inclusion. Very close to the inclusion they tend to become parallel to layering. The inclusion does show a conformity of its edge with the slight step formed in the outer layer by movement along a fracture (Figure 7, point a). The calcite twin lamellae spacing index, measured for domains in a limestone inclusion along the contact with the outer layer, show the highest value (137) opposite the point where the fracture terminates. Values in other domains fall off to roughly half this. In a specimen loaded to stage 1, no corresponding change in the index along the inclusion is seen.

Microscopic examination of the outer layers adjacent to an inclusion reveals that microfractures are concentrated near the acute apex between the fracture and the inside of an outer layer (Figure 7). The existence of a microfracture concentration (Figure 7, arrow) outside the fringe of microfractures along either side of the shear fracture suggests that the differential stresses were not homogeneous throughout the outer layer adjacent to the inclusion shortly before or during failure. In all specimens examined in thin section, microfractures were oriented parallel or sub-parallel to the maximum load direction.

Using the experience gained in detecting incipient failure from the force-displacement plot during stage 2 tests, a few specimens were loaded to within a few percent of their initial failure strength (stage 1 test). A pattern of microfracturing very similar to that seen in stage 1 specimen, only without the fracture, is seen (Figure 7). Sites of probable incipient failure, consisting of 'en echelon' microfractures arranged along narrow linear zones of potential shear failure, are mapped (Figure 8). Accompanying these zones are microfracture concentrations

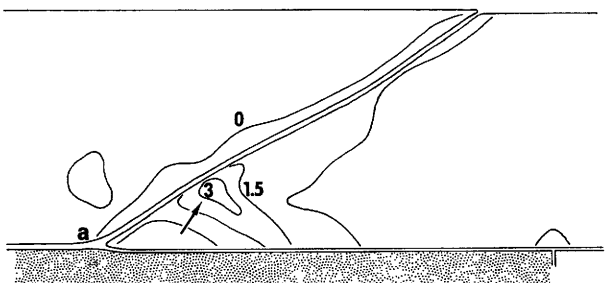

Figure 7. Portion of an outer layer in stage 2 specimen containing a limestone inclusion, shortened at 1.0 kb. Diagonal opening is initial fracture. Contours show microfracture density as the average number of microfractured grains crossed per millimeter of traverse.

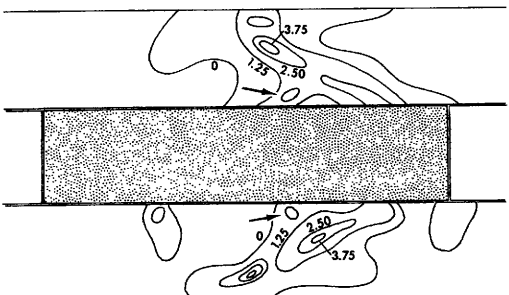

Figure 8. Schematic diagram of the central portion of a stage 1 specimen containing a limestone inclusion (stipled), shortened at 1.0 kb confining pressure. Contours show microfracture density as the number of microfractured grains crossed per millimeter of traverse.

(Figure 8, arrows) corresponding in position to that seen outside the shear fracture zone in Figure 7. This pattern occurs on both sides of the specimen. It is apparent that the differential stress required for grain fracture is reached in other areas near the inclusion apart from the zone along incipient macroscopic shear fractures. It would seem reasonable to suggest that the microfractures occurring outside the site of macroscopic shear fracture are developed at least at the same time as development of the initial fracture and perhaps earlier. This is consistant with the development of precursive microfractures prior to macroscopic failure of cylindrical laboratory specimens (Friedman, 1975).

Tests loaded to stage 3 exhibit considerably more complex deformation. However, for the three specimens subjected to this degree of loading, there was an overall similarity in fracture configuration (plate 3). One outer layer of each specimen contains intersecting fractures while the other outer layer always contains nonintersecting fractures. Fracture-bounded trapezoids or wedges are translated perpendicular to the shortening direction, toward or away from the center of the specimen, depending on the configuration of component fractures. This relatively large scale cataclasis results in a thickening of the specimen about the inclusion. At the same time the inclusion deforms to take up the new shape given to the inclusion cavity by movement of the wedges. The distribution of microfractures in a stage 3 specimen is relatively diffused (Figure 9a), but it does bear some resemblance to that developed at stage 2.

Two of the stage 3 specimens were loaded to initial failure and removed for observation before being reloaded to the final degree of shortening. The consistent pattern of shear fractures for the initial failure

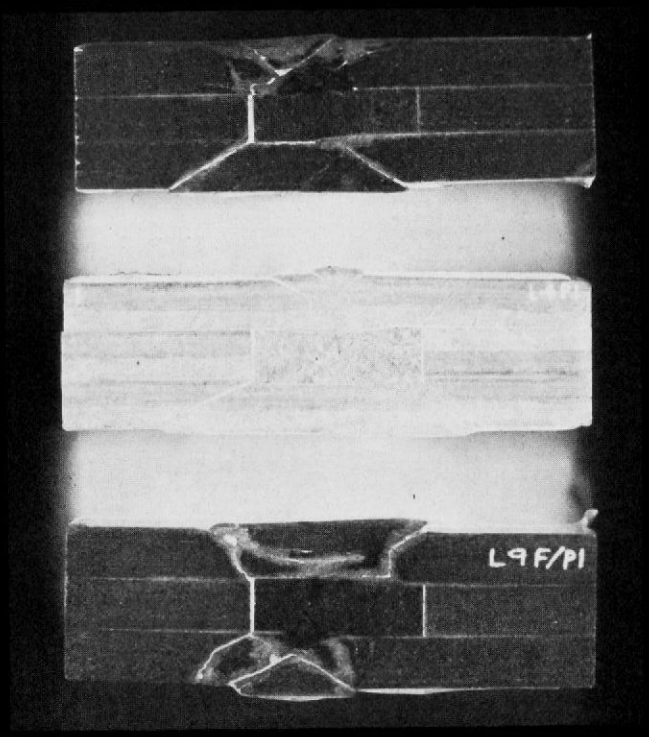

Plate 3. Stage 3 specimens containing limestone inclusions, deformed at 1.0 kb.

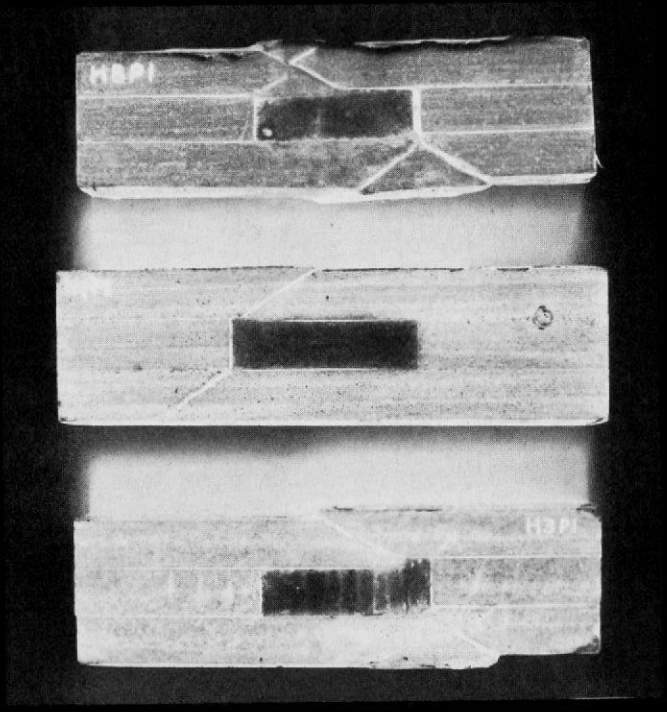

Plate 4. Stage 2 (center) and stage 3 (outside) specimens containing halite inclusions, deformed at 1.0 kb.

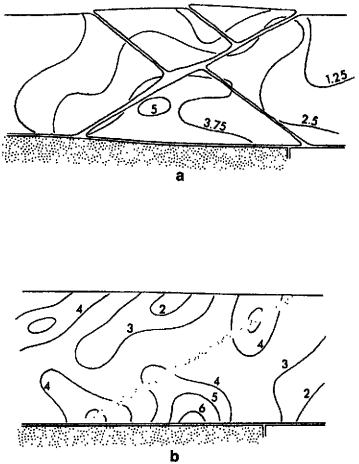

Figure 9. Portions of an outer layer in limestone-cored specimens shortened to stage 3. Diagram a shows deformation at 1.0 kb confining pressure; diagram b shows deformation at 2.0 kb confining pressure. Contours show microfracture density as the average number of microfractured grains crossed per millimeter of traverse.

was recorded so that the relative position of new fractures could be determined. In both specimens one of the new fractures is in line with an original fracture. Also a new fracture intersects the inclusion at a corner. In the specimen loaded only once to stage 3, fractures corresponding to all these positions are present.

Halite inclusion. Initial failure in specimens containing polycrystalline halite inclusions also consists of a single fracture in each outer layer. The two are parallel, but they always intersect the inclusion at or very close to a corner (Plate 4). A distribution of microfractures like that observed in limestone-cored specimens is not seen, rather microfractures are restricted to the narrow zone along the fractures. In contrast to the limestone-cored specimens, the influence of the stress concentrations opposite the inclusion corners has become dominant in localizing deformation. In stage 3 tests, subsequent fracturing continued to be localized mostly at corners.

The stage 3 portions of force-displacement curves for limestone and halite-cored specimens are very similar in character (see Figure 5). After the stress drop for initial failure is reached (approximately 0.25-0.5 kilobars), a series of gentle rises terminated by drops less rapid but of about the same magnitude as the initial drop occur. These subsequent drops probably accompany formation of new fractures.

Tests at 2.0 kb

In specimens loaded at a confining pressure of 2 kb. deformation continues to be localized adjacent to the inclusion but is more uniformly distributed than at 1.0 kb. (Figure 9, Plates 5, 6). In both limestone and halite-cored specimens, flow occurs along shear zones in contrast to

failure along discrete fractures as at 1.0 kb. (Figure 5). Microfracturing becomes the dominant deformation mechanism and is in large part responsible for the loss of ability to sustain an increasing differential stress. Again, the microfracturing is visible in hand specimen and unaided observation gives a good estimate of its extent.

The deformation in specimens having limestone and halite inclusions is similar enough to obviate separate discussions for each. With either type of inclusion, the distinction in thin section between stage 1 and stage 2 tests is not possible because the microfracture intensity does not change significantly between these stages of loading. Stage 2 tests produce microfracture distributions occupying the full width of an outer layer although the distribution tends to narrow in lateral extent away from the inclusion. In hand specimen, indistinct narrow shear zones are visible that often intersect the inside of an outer layer just beyond the inclusion. They coincide approximately with the lateral extent of the microfractured zone (Figure 10, stippled zones).

In the two stage 3 specimens run for each inclusion type, shear zones with visible offset form. They are oriented and located similarly to those in stage 2 tests run at 1.0 kb. (Plate 5, arrows). Shear zones having the same geometry as those in stage 2 tests are not seen. They may have been formed and then obliterated by continued cataclasis. Most noticeable is the thickening, by microscopic cataclasis, of the outer layers over the inclusion (Plate 5). This is most extensively developed in limestone-cored specimens where the thickening gradually increases to a point (roughly) over the center of the inclusion. In halite-cored specimens thickening is more abrupt and more laterally restricted. (Plate 6).

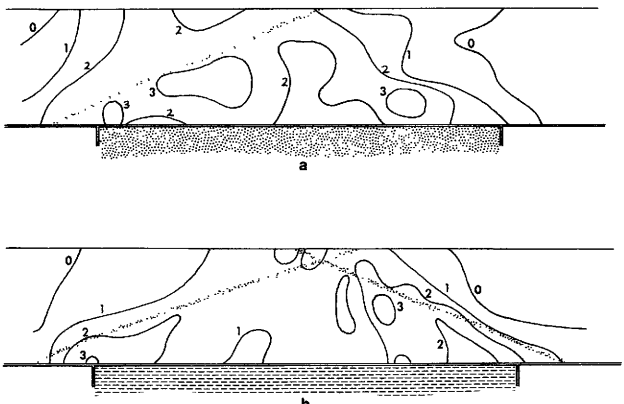

Figure 10. Outer layers in limestone-cored (a) and halite-cored (b) stage 2 specimens deformed at 2.0 kb. Narrow stipled zones represent early shear zones. Contours show microfracture density as the average number of microfractured grains crossed per millimeter of traverse.

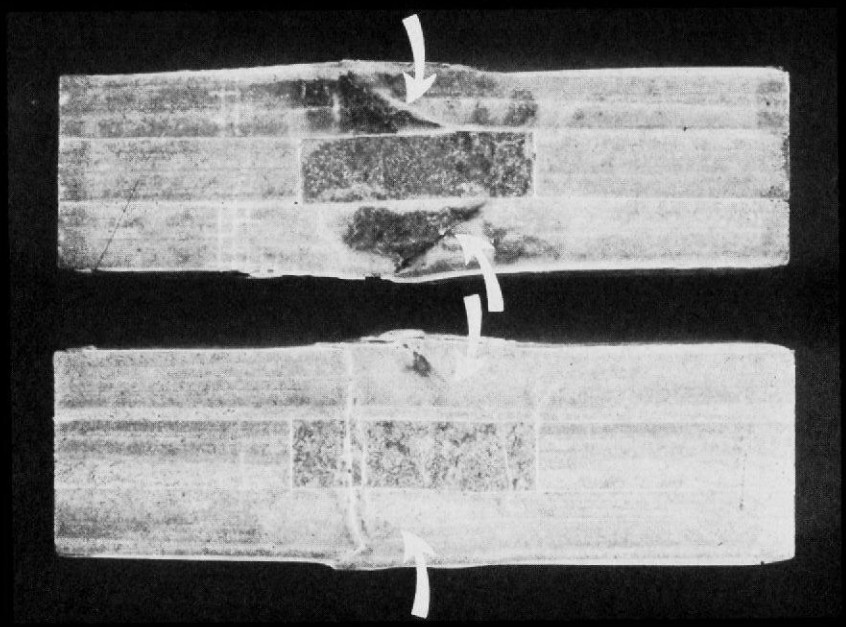

Plate 5. Stage 3 specimens containing limestone inclusions, deformed at 2.0 kb. Arrows point to shear zones.

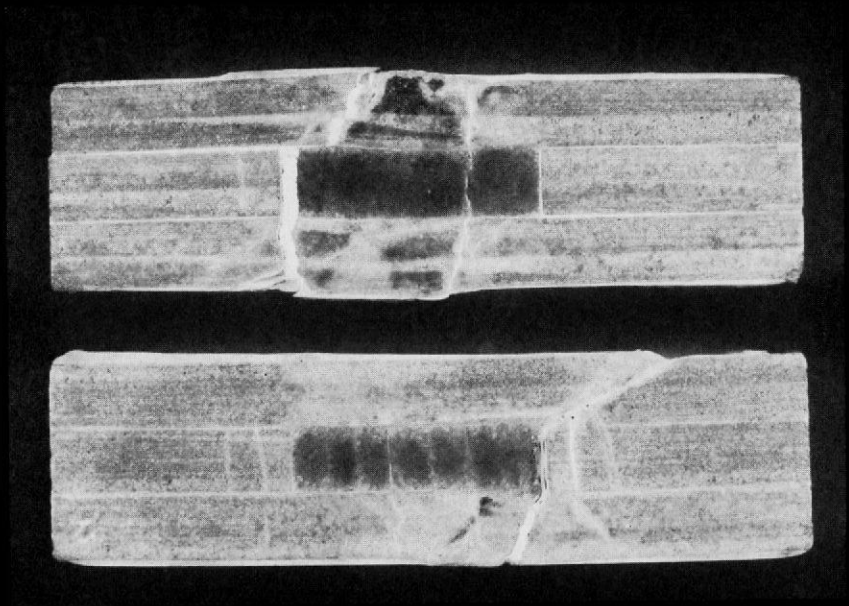

Plate 6. Stage 3 specimens containing halite inclusions, deformed at 2.0 kb.

The limestone inclusions appear to be only slightly thickened and are slightly sigmoid in shape laterally (Plate 5). The expected thickening may be taken up by pore collapse. Thickening in halite inclusions is pronounced but confined to areas opposite the areas of thickening in the outer layers (Plate 6).

Microscopic examination of the outer layers. Density of microfracturing was mapped in the outer layers with the intention of comparing their distribution to that seen in the 1.0 kb. specimens. Most of the area over the inclusion in each specimen is microfractured to some degree. The limit of microfracturing forms a roughly trapezoidal shape centered over the inclusion and broadening toward it (Figure 10). Areas of high microfracture concentration cover larger areas than in 1.0 kb. specimens but the microfracture density is no higher than that seen in 1.0 kb. specimens (compare Figures 7, 9, and 10).

Microfracture distributions are symmetrically related to the position of the inclusion for both lithologies in stage 2 test specimens (Figure 10). Of greatest interest is the fact that most of the higher concentrations of microfractures occur in from the ends of the inclusion rather than at the corners. The shear zones developed at stage 2 may form just after the microfracture concentrations. These shear zones bound the outside edges of the areas of highest concentration. In these specimens, the gradient in microfracture concentration toward the center of an outer layer is sharp enough to allow an intact portion to move past a highly microfractured portion along a narrow shear zone. Shear zones like those developed at stage 3 may be localized by the microfracture concentrations themselves. The fact that microfracturing is widespread suggests that it must be the initial mode of failure. On the scale of the specimen a zone

of localized shear alone would probably tend to prevent the differential stress from increasing to a level conducive to wide zones of microfracturing.

Microfracture distributions in stage 3 specimens show high concentrations in places similar in position to those at stage 2. The overall pattern, however, is much more complex and microfracture densities are up to twice as high.

Tests at 3.0 kb.

The difference between the deformation seen in the outer layers of limestone and halite-cored specimens becomes almost indistinguishable at 3.0 kb. Pervasive cataclasis is the dominant deformation mechanism under these conditions. The force-displacement curves (Figure 6) suggest work hardening is taking place and it is no longer possible to distinguish stage 1.

Stage 2 tests produce zones of pervasive microfracturing occupying all of the outer layer over an inclusion. These zones are easily visible in hand specimen (Plate 7). In stage 3 specimens, the extent of microfracturing is about the same with a thickening of the outer layers apparent over the inclusion. A faint shear zone is apparent in one halite-cored specimen, the zone bounding one side of a microfractured zone.

Microscopic examination of the outer layers. Outer layers in one stage 2 specimen and one stage 3 specimen are mapped and show microfracture concentrations located near, but not at, the inclusion corners (Figure 11). Also, microfracture densities are no higher than those in 1.0 kb., stage 2 specimens.

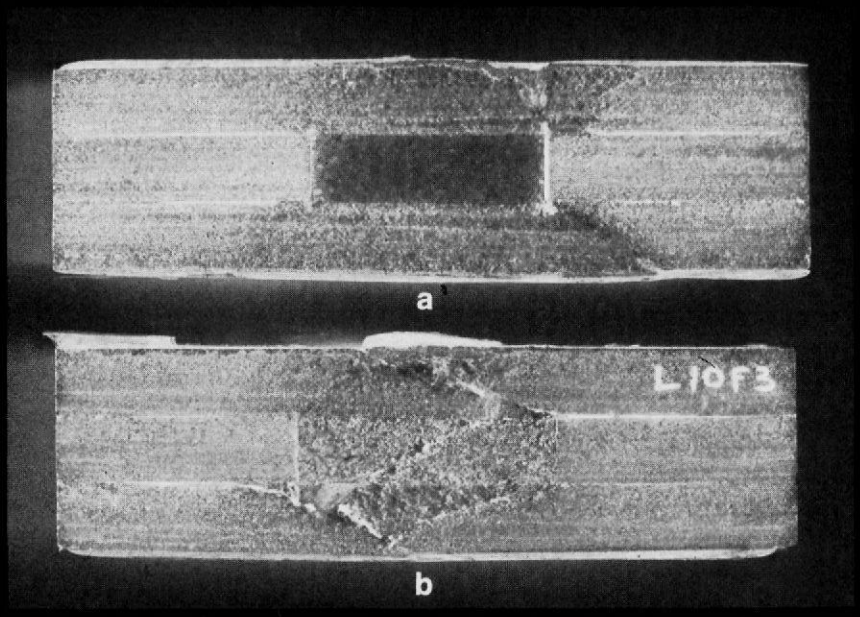

Plate 7. Stage 2 specimens containing halite (a) and limestone (b) inclusions, deformed at 3.0 kb.

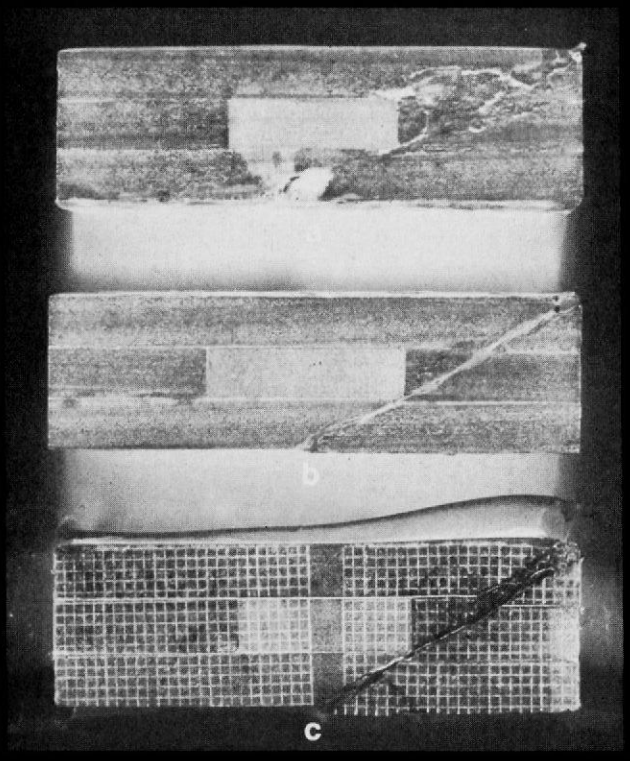

Plate 8. Stage 2 specimens containing inclusions of Tennessee Sandstone, deformed at 1.0 kb (a) and 2.0 kb (b, c).

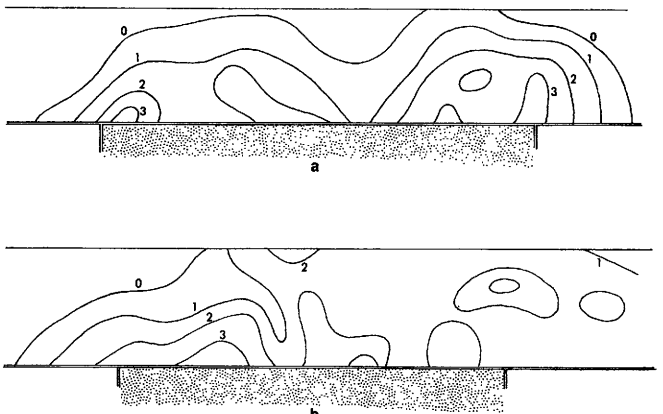

Figure 11. Outer layers in limestone-cored specimen deformed at 3.0 kb. Diagram a shows stage 3 deformation and diagram b shows stage 2 deformation. Contours show microfracture density as the average number of microfractured grains crossed per millimeter of traverse.

Tests on specimens having inclusions of Tennessee sandstone

Three specimens containing inclusions of Tennessee sandstone were deformed to determine the effect of having a material with a higher failure strength than Coconino sandstone as the inclusion. At 1.0 kb. a through-going fracture or, at 2.0 kb. a shear zone forms that comes close to an inclusion corner (Plate 8). Very faint linear markings inclined at close to 45 degrees to layering (perhaps Luders' bands, Friedman and Logan, 1973) are seen in the Coconino segments of the central layer. It is difficult to say if the fracturing is localized by the inclusion corner. Because of the specimen geometry a through-going shear fracture must pass very close to an inclusion corner in any case if it is to be contained solely in Coconino sandstone.

Tests on specimens having clay inclusions

To approximate a material having no shear strength in the position of the inclusion, two tests were conducted using modelling clay ("plasticine"). The purpose was to find if the absence of an inclusion had any effect on deformation. A specimen jacket allowing the admission of the confining medium through the inclusion site would have been ideal but technical difficulties preclude this. The modelling clay was found to be virtually incompressible at 1.0 kb. because no indentations were seen on the jacketing material after the tests. Further, the clay probably has a shear strength much lower than that of halite because, unlike halite, it penetrates between the specimen layers during the test.

Both specimens were loaded to initial failure and contained one or two fractures in each outer layer , over or projecting into the inclusion

(Plate 9). While the fractures did seem to be localized over the inclusion, they showed no consistent geometry or position and individual fractures were highly variable in orientation.

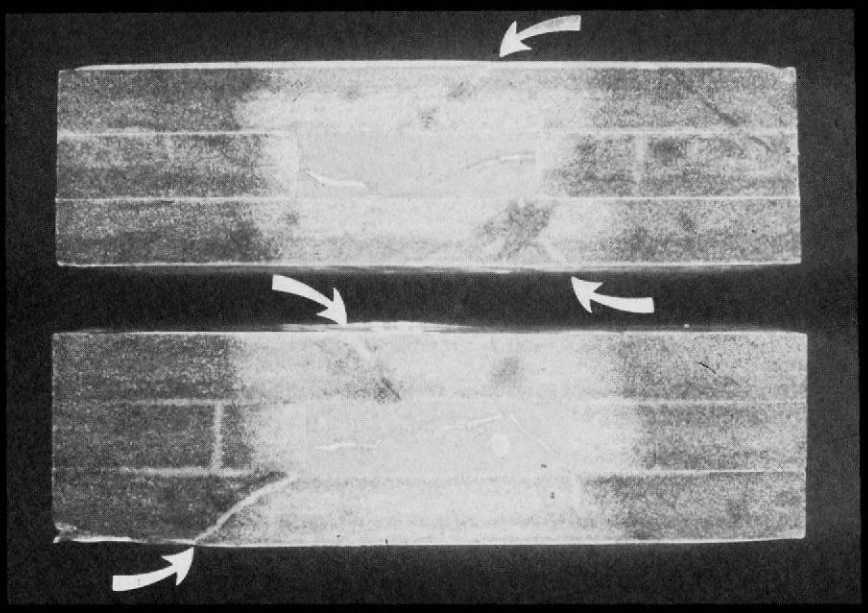

Plate 9. Stage 2 specimens containing inclusions of modelling clay, deformed at 1.0 kb. Arrows point out fractures.

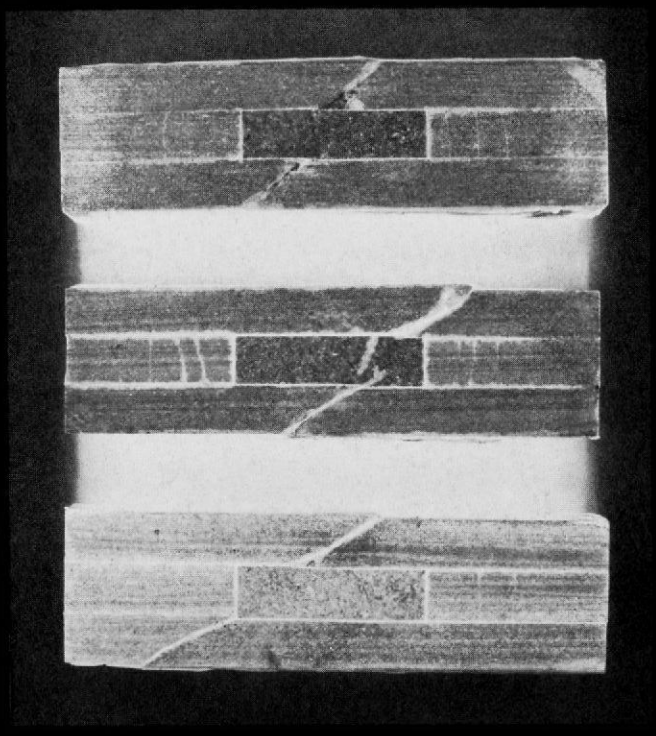

Plate 10. Stage 2 specimens containing limestone inclusions which have been lubricated on the sides in contact with the outer layers and deformed at 1.0 kb.

ANALYSIS OF EXPERIMENTAL RESULTS

Preliminary analysis of experimental results

Most apparent from the results is the consistent way in which deformation is localized in the outer layers at all confining pressures. Microfracturing in specimens containing limestone inclusions is concentrated in areas near, but not at, the corners of the inclusions. Macroscopic fractures and shear zones seem to show a distinct spatial relation to these concentrations. It is also apparent that the type of inclusion is important in controlling fracture position relative to the inclusion. Limestone and halite inclusions appear to exert a definite control on fracture position and geometry while clay does not. The results with a Tennessee sandstone inclusion are inconclusive.

These observations suggest that in some way the manner in which the inclusion deforms is an important factor in controlling deformation of the outer layers. In the case of inclusion materials that have lower strengths relative to Coconino Sandstone this likelihood appears to be greatest for the least ductile material. Limestone inclusions appear to exert the strongest influence in that the outer layer deformation is most reproducible but is not localized by inclusion corners.

The following tentative hypothesis explains the position of macroscopic fractures in specimens cored with halite. A high stress concentration should exist in the outer layers opposite the corners of the inclusion if the inclusion can support a shear stress against the boundaries between the two materials of the middle layer. With a halite inclusion, this stress concentration would be highest when the halite yields

and its Poisson's ratio becomes 0.5. The stress concentration is high enough to localize the macroscopic shear fractures. Similar shear fractures do not form at the same place in specimens containing limestone cores, possibly because the mechanical contrast between the limestone and sandstone is not as great. Because a corner stress concentration cannot explain deformation associated with limestone inclusions, they were subjected to further analysis. It was initially assumed that some aspect of the deformation of the inclusion was most important in localizing the deformation in specimens cored with limestone.

Limestone inclusion analysis

Direct surface strain measurement. The results of the grid measurements on four limestone inclusions are plotted in Figure 12. The graphs show strain in the direction parallel to loading at regularly spaced intervals. The high degree of irregularity in the plots may stem from the indistinct nature of the grid lines. However, both sets of measurements show the same overall pattern: the inclusions measured have shortened roughly twice as much at the ends as in the middle.

Internal strain measurement. Measurements of twinned calcite grains were made using the Groshong (1972) technique but were uninterpretable because of scatter and too few data. The reason may be that the inclusions were subjected to at least two sets of orientations of the principal stresses. The first would result from the application of the confining pressure because only two sides of an inclusion are in direct contact with the confining fluid. The second set of directions would result from application of the piston load. The Groshong technique assumes non-rotational stress. Enough grains per domain were not available to distin-

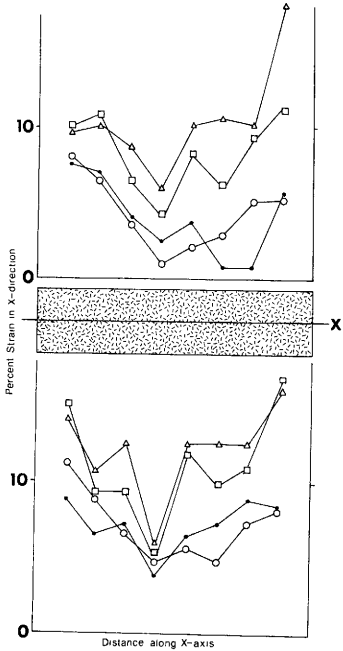

Figure 12. Lateral strain in percent from measurements of distorted grids on four limestone inclusions from stage 3 experiments (arbitrary symbols used to allow distinction between specimens). Horizontal axis represents distance along line superimposed on inclusion face between graphs. Strains in upper diagram are calculated by the rosette method. They are for the axis of greatest shortening which may or may not be parallel to X. Those in the lower diagram are calculated by direct measurement parallel to X.

guish two maximum principal stress orientations in the manner of Teufel (1975). It was noted, however, that the abundance of calcite twin lamellae (average of number of twin lamellae per millimeter when viewed on edge in all grains measured in any domain) in the end domains of inclusions was 20 to 40 percent greater than that in the central domain.

Elastic solution for inclusion deformation. In an attempt to substantiate the results of the previous two forms of strain analysis, a theoretical analysis for infinitesmal elastic strain is performed on a lateral cross-section of an inclusion using traction boundary conditions. The method is fundamental to the theory of elasticity and is well explained by Timoshenko and Goodier (1970). To determine how a perfectly elastic body will deform, boundary stresses must be specified that will maintain the body in equilibrium. However, the problem remains statically indeterminate until the elastic deformation of the body is considered. The components of strain are defined in terms of the two displacement functions u and v. They cannot be taken arbitrarily because a certain relation exists between the strain components. This relation, called the condition of compatibility, must be satisfied in order to find u and v.

While the deformation of the inclusion may be largely of a non-elastic sort, this solution is intended only as an indication of how the inclusion might begin to deform. In the earliest stages the deformation is probably essentially elastic. The details of the solution are given in the appendix.

Boundary conditions: The shear stress boundary conditions (τxy) are arrived at using deformational characteristics of the specimen materials and properties resulting from the symmetry of the specimen. The normal

stress boundary conditions (σ_x, σ_y) are assumed to be approximately uniform distributions of the confining pressure and differential loads.

To simplify the assignment of shear stress boundary conditions, the analysis was restricted to one quarter of the cross-section, i.e., one of the parts bounded by the two perpendicular center lines and the edges of the inclusion (Figure 13). By symmetry operations the solution is then extended to determine the deformation field of the whole cross-section. Using the center lines allowed the simplification of setting the shear stress equal to zero along the two sides of the figure that coincide with the two center lines. No shear stress is assumed to operate along these lines because they lie halfway between edges of the inclusion on which equal shear stresses are assumed to be operating in the same direction.

Shear stresses operating on the outsides of an inclusion are assumed to be zero at the center of any side and increase toward any corner. During a test, the sides of the inclusion against the outer layers probably shorten more than the initial equivalent adjacent length of an outer layer. This occurs because most of the shortening in an outer layer is probably more evenly distributed along its entire length. Comparison of stress-strain curves for Coconino sandstone and Indiana limestone given in Handin, et al. (1972) show a greater ability for the limestone to shorten for a given differential stress. Greater shortening in the limestone would result in a shearing force between it and either sandstone layer.

For these frictional forces to be generated, interlayer displacement is required between all components of the middle layer and either outer layer. Possible evidence for this exists in the form of extension frac-

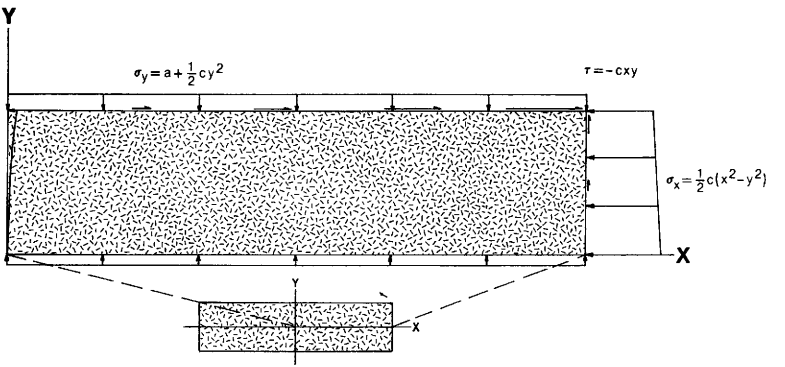

Figure 13. Two-dimensional portion of inclusion considered in elastic analysis, showing arbitrary but correctly proportioned boundary conditions. Inset shows portion of inclusion analysed.

tures oriented parallel to the specimen ends that occur in both lithologies of the central layer (See Plate 10). An explanation for these fractures assumes slip takes place between the layers. On decrease of the differential load at the end of a test, stored elastic strain in the outer layers is released. The central layer probably has not experienced as high a load as the outer layers because of its overall less rigid constitution and so stored elastic strain is less. Friction between the layers allows the expansion of the outer layers to put the segments of the central layer into extension, perhaps even into tension. Interlayer slippage may still take place but the friction required to put any portion of the central layer into extension or cause failure in tension would be relatively small. These fractures seem to be found mostly in one kilobar specimens. A few two kilobar specimens contain them, but none of the three kilobar specimens do. The phenomenon may not be so common in the higher confining pressure specimens because of the pervasive cataclasis which would prevent the outer layers from storing the needed elastic strain.

Results of elastic solution

Displacement functions and lateral strains are plotted for arbitrary values of the boundary conditions and elastic constants. Strain parallel to the differential load direction (x-direction) is shown in Figure 14b. Displacements or the shape that the block is calculated to assume are shown in Figure 14a. A comparison with the strains parallel to x calculated from surface measurements shows good agreement with the theoretical calculation in that lateral strains are considerably higher at the ends

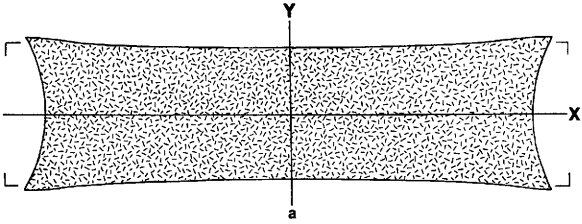

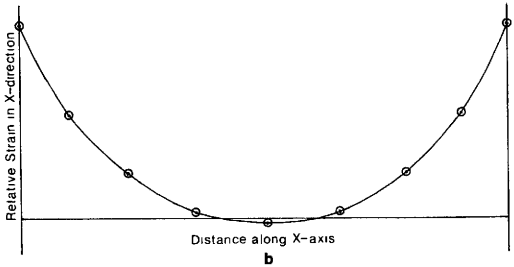

Figure 14. Theoretical inclusion deformation. Diagram a shows, in exaggerated form, the shape the inclusion assumes under arbitrary values of the given boundary conditions. Note thickening of the ends. Diagram b shows the theoretical equivalent to the strain distribution shown in Figure 12. Only relative values are shown.

than in the middle. Figure 14a shows the block to thicken at the ends. This is remarkable when compared to the intuitive belief that the block should have thickened most in the middle, but it seems reasonable in the light of the assumed boundary conditions, (i.e., shear stress increasing toward the ends of the inclusion). If the block in reality is shortening most at the ends, as suggested by measurement and theory, then it would be reasonable to expect a resulting expansion at right angles to the differential load direction, based on the Poisson effect. In summary, the elastic solution predicts the same distribution of deformation given by the visual and optical measurements.

INTERPRETATION OF ANALYSIS

A spatial relation exists between the position of deformation in the outer layers and the deformation of the limestone inclusion. The microfractures, which cluster on the inside of the outer layers in areas near the ends of the inclusion, are located over the areas of the inclusion which have been shown to be shortening the most.

It is thought that the initial deformation in the form of microfracturing may be controlled and localized by the adaptation of the outer layers to the deformed shape taken on by the limestone inclusion. Greater expansion of the ends of an inclusion perpendicular to the load direction results in two crests separated by a trough to which an outer layer must conform (Figure 15). This results in a folding of the outer layer. The amplitude of this folding is estimated to be approximately 0.01 cm. (See Appendix). The superposition of compressive bending moments in these folds on the load produced directly by the pistons results in stress concentrations high enough to locally exceed the failure strength of individual sandstone grains (Figure 15). A limestone inclusion does not produce a stress concentration opposite an inclusion corner that is strong enough to cause microfracturing.

A stress concentration will depend on the tendency for a "step" to form in the boundary between the outer and middle layers due to a contrast in the Poisson's ratio between the two lithologies of any specimen. A frictional restraint against expansion of the inclusion ends is imposed by the contact of the inclusion ends with the adjoining sandstone segments. This restraint restricts the formation of a step. Most favorable

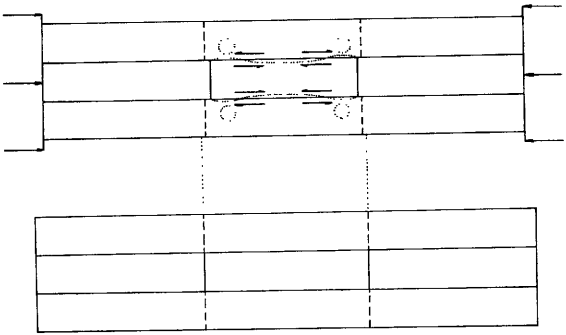

Figure 15. Schematic depiction of deformation in a specimen containing a limestone inclusion. Single-barbed arrows show sense of shear set up as inclusion shortens more than the equivalent original length of an outer layer. Sinuous dotted lines show deformed inclusion shape (exaggerated). The dotted circles show areas of stress concentration. It is assumed that the extreme ends of the inclusion remain at the same thickness as the sandstone segments of the middle layer.

for the formation of such a step would be a material having a high Poisson's ratio and relatively low shear strength. Halite inclusions fit these requirements most closely. With clay the shear strength is negligable. The relatively high shear strength of the limestone retards the formation of a step. Instead the inclusion takes on a shape approximated by the dotted lines shown on Figure 15.

The behavior of the limestone inclusion is thought to be controlled largely by the shear stress assumed to operate along the contact between the inclusion and the outer layers (Figure 15). To test the significance of this shear stress, an attempt was made to reduce it by lubricating the contact with molykote (a commercially prepared molybdenum disulphide lubricant). In three experiments performed at 1.0 kb. and carried to stage 2, one fracture in each outer layer forms. Both are always in line with one another. In one case, one of the fractures intersects the inclusion at a corner (Plate 10). All three lubricated specimens are roughly 20 percent stronger at failure than the nonlubricated ones.

From the change in fracture geometry (V-shape to in-line), the weak tendency for fractures to intersect inclusion corners and the increased strength, it is apparent that shear stress along the inclusion sides may be an important boundary condition. Reducing it is expected to decrease thickening of the inclusion ends which in turn should reduce the ability of the inclusion to fold the outer layers. The associated stress concentrations would then be reduced, perhaps enough to curtail formation of the microfracture concentrations which seem to nucleate the initial macrofractures and so reduce the failure strength.

One specimen containing a continuous central limestone layer, loaded

to stage 2 at 1.0 kb., has a failure strength roughly the same as that for lubricated specimens. With both the sandstone and limestone layers being shortened the same amount, essentially no shear stress is assumed to develop along the layer contacts. It appears that for the lubricated specimens and the solid-limestone-layer-specimen, the sandstone layers remain intact up to the time of failure. Indeed, thin section examination of the outer layers in lubricated specimens indicates that no microfractures whatsoever are formed except for those immediately along the trace of the macrofractures.

Processes controlling deformation subsequent to initial failure or yield probably change markedly. Shortening is no longer being taken up elastically and so the boundary conditions proposed for the pre-failure stage no longer apply. Relief of the shear stresses between the inclusion and outer layers may take place as further shortening is taken up by movement on macro- or microfractures. The influence of these shear stresses on fracture position was demonstrated previously by lubrication of the inclusion-outer layer contact. Subsequent fractures in limestone-cored specimens that meet inclusion corners may be localized by corner stress concentrations. With the relief of the shear stresses, the thickening effect postulated for limestone inclusions in intact specimens is no longer operative, leaving only the corner effect to produce stress concentrations in the outer layers.

CONCLUSIONS

Deformation in specimens

An inclusion of contrasting lithology in a three layer specimen appears to have an influence on the style and position of deformation as follows:

a. Deformation in the outer layers, whether in the form of macroscopic shear fractures, microfracturing or pervasive cataclasis, is localized over the inclusion in specimens cored with halite and limestone. This localization also occurs if the inclusion is moved toward one end of the specimen. While macroscopic fracturing is localized over clay inclusions, it does not show a reproducible geometry as seen with halite or limestone inclusions.

b. Deformation in the outer layers produced by shortening a specimen to stage 2 is localized at inclusion corners in specimens cored with halite and inward from the corners in specimens cored with limestone. Specimens with limestone or halite inclusions that are shortened to stage 3 continue to show localized deformation. However, spatial relations become important because pre-existing fractures appear to localize subsequent ones.

c. Microfractures in quartz grains of the outer layers are usually concentrated in zones next to the inclusion, inward from the corners. Macroscopic fractures and shear zones appear to be immediately adjacent to, or coincident with, these zones.

d. Lubrication of the contact between limestone inclusions and the outer layers causes a change in the macroscopic shear fracture geometry in specimens shortened to the initial failure point. The microfracture

concentrations are not developed. Also, the failure strength increases.

e. With an inclusion that has a greater failure strength than Coconino Sandstone (i.e. Tennessee Sandstone), deformation is restricted to the end-thirds of the specimen.

Mechanism by which deformation is localized in the specimens

As a specimen is compressed, an inclusion composed of a material that shortens more under a given load than the outer layers, here Coconino Sandstone, experiences more shortening than the same original adjacent length of sandstone (Figure 15). This process generates shear stresses along the inclusion-outer layer contact. These shear stresses are important in localizing deformation if the inclusion shortens more than the enclosing material under the same stress but is still capable of supporting a relatively high shear stress.

The shear stresses are important because they appear to cause thickening of the ends of limestone inclusions. The folding of the outer layers as they conform to the new shape of the inclusion results in local stress concentrations in the outer layers away from the inclusion corners. These stress concentrations nucleate macroscopic fractures or shear zones. In their early stages, these lines of failure do not have corresponding extensions into the inclusion. The initial V-shaped shear fracture pattern may result from a tendency towards a condition of least work, i.e. fractures in line would require the establishment of a shear zone through the inclusion.

Reducing the shear stresses by lubrication changes the deformational style in the outer layers. A halite inclusion has much the same effect

by virtue of its relatively low ability to support a shear stress. Clay inclusions represent the closest approximation to a material having no shear strength. In this case deformation is only localized because of the weaker cross section that lies through the inclusion. An inclusion having a higher failure strength than the Coconino Sandstone will force fractures to pass through all three Coconino Sandstone layers. In general, the contrast in the ability of the inclusion and surrounding material to support a shear stress controls the position and style of deformation. For deformation to be localized, the Poisson's ratio of the inclusion must be higher than and the relative strength lower than that of the surrounding material.

Speculations on the application of the experimental results to natural deformation

A mechanism depending on deformational properties of specimen materials explains the localization of the initial deformation in the experiments. While the symmetry of the specimens doubtless has an effect on the geometry of the deformation (i.e. the location of the inclusion in the center of the middle layer allows the assumption of zero shear stress at the center of the inclusion-outer layer contact to be made), boundary conditions operating in the specimens could be expected to operate for similar reasons at natural facies changes. The apparent lack of importance of the inclusion corners is noteworthy in that such a counterpart in nature may not be necessary to localize deformation. Simply a shear stress operating as a result of differing mechanical properties along the horizontal contact between two different lithologies of a lateral contrast

may be enough to localize deformation in a manner similar to that postulated for the specimens. Put another way, a very abrupt lateral contrast would not necessarily be required to produce this mechanism.

The experimental results have also assisted in clarifying thinking on the origin of White Uplift. There, a major reverse fault bounds one side and dips beneath the core. It is known to transect the Precambrian sedimentary basement. Perhaps processes which localize deformation in the specimens have operated beneath the carbonate build-up at the site of White Uplift to develop this fault. Subsequent movement along it has then partly resulted in the structural expression given to the carbonates and Precambrian material we now see.

Most speculative is the suggestion that the localization mechanism operating within the specimens may act to nucleate thrust faults. The major thrust belts of North America are located in sedimentary basins containing numerous facies changes. Possible stress concentrations associated with the facies changes may act to initiate fractures which propagate to form a potential thrust fault.

It cannot be emphasized too strongly that these speculations are intended only to suggest features to look for in the field. As stated at the beginning of this thesis, facies changes are relatively common in regionally deformed sedimentary sequences. Only examination of the structural fabric at such facies changes on all scales will provide any clue as to whether the findings in this thesis offer any explanation for features seen in nature.

APPENDIX

Solution of elastic boundary value problem

A polynomial solution for the differential equation

$$\frac{d^4\phi}{dx^4} + 2\frac{d^4\phi}{dx^2dy^2} + \frac{d^4\phi}{dy^4} = 0 \quad , \qquad 1.$$

where ϕ is the Airy stress function and x and y are coordinate axes, was found by a process of elimination of arbitrary constants from a polynomial of order sufficient that terms would survive fourth order differentiation. The only strict requirement imposed for boundary conditions for the purpose of obtaining the solution was that the shear stress along two adjacent sides of the rectangular strip representing the quarter of the inclusion be zero. Arbitrary shear and normal stresses for the other sides were allowed as long as they corresponded to the conditions expected. The details of solution for two-dimensional rectangular strips are given by Timoshenko and Goodier (1970) and Chapple (1968).

The stress function found was

$$\phi = \frac{1}{2}ax^2 + \frac{1}{4}cx^2y^2 - \frac{1}{24}by^4 .$$

Substituting this back into equation 1. gave

$$c - b = 0 .$$

For ϕ to satisfy equation 1. it is necessary that $b = c$. This condition was applied to the boundary conditions.

The boundary conditions obtained are

$$\sigma_x = \frac{d^2\phi}{dy^2} = \frac{1}{2}c(x^2 - y^2)$$

$$\sigma_y = \frac{d^2\phi}{dx^2} = a + \frac{1}{2}cy^2$$

$$\tau_{xy} = -\frac{d^2\phi}{dxdy} = -cxy$$

where σ_x and σ_y are the normal stresses acting parallel to the x and y directions respectively, τ_{xy} is the shear stress acting in the xy plane, and a and c are arbitrary constants allowing assignment of stresses.

Solving Hooke's Law for strains,

$$e_x = \frac{1}{E}(\sigma_x - p\sigma_y) = \frac{1}{E}((\frac{1}{2}c(x^2-y^2)) - p(ax+\frac{1}{2}cy^2)) \qquad 2.$$

$$e_y = \frac{1}{E}(\sigma_y - p\sigma_y) = \frac{1}{E}(ax+\frac{1}{2}cy^2 - p(\frac{1}{2}c(x^2-y^2))) \qquad 3.$$

$$\gamma_{xy} = \frac{1}{G}\tau_{xy} = -\frac{1}{G}cxy$$

where e_x and e_y are the elongations in the x and y directions respectively, γ_{xy} is the shearing strain in the xy plane, p is Poisson's ratio, E is Young's modulus and G is the shear modulus.

In terms of displacement u in the x-direction and v in the y-direction,

$$e_x = \frac{du}{dx},\quad e_y = \frac{dv}{dy},\quad \gamma_{xy} = \frac{du}{dy} + \frac{dv}{dx}.$$

Integrating equation 2. with respect to x and equation 3. with respect to y,

$$u = \frac{1}{E}(\frac{1}{6}cx^3 - \frac{1}{2}cxy^2 - pax - \frac{1}{2}pcxy^2) + f(y)$$

$$v = \frac{1}{E}(ay + \frac{1}{6}cy^3 - \frac{1}{2}pcx^2y + \frac{1}{6}pcy^3) + f(x)$$

where f(y) and f(x) are unknown functions of y and x respectively that must be included in order to take into account γ_{xy}. Substituting u and v into the expression for γ_{xy} in terms of displacements,

$$\frac{du}{dy} = \frac{1}{E}(-cxy - 2pcxy) + \frac{df(y)}{dy}$$

$$\frac{dv}{dx} = \frac{1}{E}(-2pcxy) + \frac{df(x)}{dx}$$

However, no terms in x or y only exist so that $\frac{df(y)}{dy}$ and $\frac{df(x)}{dx}$ can only

be expressed as arbitrary constants m and n. Integrating,

$f(y) = my + j$, $f(x) = nx + k$.

Conditions of constraint:

At $x = 0$, $y = 0$; $u = 0$, $y = 0$; therefore $j = k = 0$.

Also $\frac{du}{dy} = 0$ when $x = 0$ and $y = 1$, therefore $m = 0$.

Similarly, $n = 0$.

Therefore the expressions for the displacements are

$$u = \frac{1}{E}(\frac{1}{6}cx^3 - \frac{1}{2}cxy^2 - pax - \frac{1}{2}pcxy^2)$$

$$v = \frac{1}{E}(\frac{1}{6}cy^3 + \frac{1}{6}pcy^3 + ay - \frac{1}{2}pcx^2y) .$$

An estimate of the amplitude of the outer layer folding

This estimate is obtained by limiting attention to that part of an outer layer over the end of an inclusion and assuming that the fold is a pure elastic bend. Conventional strength tests on Coconino sandstone show a shortening to failure of approximately 2% at one kilobar confining pressure (Handin, et. al., 1972). If it is considered that failure takes place first in the fold fibre undergoing greatest compression and it is assumed that the shortening required for failure in that fibre is the same as in a conventional test, than a deflection can be calculated. Using a portion of an outer layer 1.5 cm. long, the deflection required to achieve a 2% shortening in the fibre undergoing greatest compression is 0.01 cm. Of course, the deflection of this idealized portion of an outer layer is only a fraction, roughly half, of the total deflection of the complete fold. Moreover, the beam is subject to the piston load which reduces the compressive bending moment required to produce failure. Therefore the calculated deflection would form an upper bound. In any

case this estimate is only used to suggest that the amplitude of the folding is very small.

REFERENCES

Blanchet, P. H., 1957, Development of fracture analysis as exploration method: Bull. Am. Assoc. Pet. Geol., v. 41, no. 8, p. 1748-1759.

Chapple, W. M., 1968, The equations of elasticity and viscosity, and their application to faulting and folding; in N.S.F. Advanced science seminar in rock mechanics, R. E. Riecker, ed., Terrestrial Sciences Laboratory, Air Force Cambridge Research Laboratories, Bedford, Massachusetts.

Cook, D. G., 1970, A Cambrian facies change and its effect on structure, Mount Stephen - Mount Dennis area, Alberta-British Columbia; in Apecial Paper No. 6, Geol. Assoc. Can., p. 27-39.

Dyke, L. D., 1972, Structural investigations in White Uplift, northern Yukon Territory; in Report of Activities, April to October, 1971, Geol. Surv. Can., Paper 72-1, Part A, p. 204-207.

Friedman, M., 1963, Petrofabric analysis of experimentally deformed calcite-cemented sandstones, Jour. Geol., v. 71, p. 12-37.

_____, 1975, Fracture in rock, Rev. Geophys. Space Phys., v. 13, no. 3, p. 352-358, p. 383-389.

Friedman, M. and Logan, J. M., 1970, Microscopic feather fractures, Geol. Soc. Am. Bull., v. 81, p. 3417-3420.

_____, 1973, Lüders bands in experimentally deformed sandstones and limestones, Geol. Soc. Am. Bull., v. 84, p. 1465-1476.

Groshong, R. H., 1972, Strain calculated from twinning in calcite, Geol. Soc. Am. Bull., v. 83, p. 2025-2038.

Handin, J., 1966, Strength and ductility, in Handbook of physical constants, S. P. Clark, ed., Geol. Soc. Am. Mem. 97, p. 223-290.

_____, Friedman, M., Logan, J. M., Pattison, L. J., and Swolfs, H. S., 1972, Experimental folding of rocks under confining pressure: buckling of single-layer rock beams, in Flow and Fracture of Rocks, Am. Geophys. Un., Geophys. Mono. 16, p. 1-28.

Jaeger, J. C. and Cook, N. G. W., 1969, Fundamentals of rock mechanics, Chapman and Hall, London

Lenz, A. C., 1972, Ordovicion to Devonion history of northern Yukon and adjacent District of Mackenzie, Can. Pet. Geol. Bull., v. 20, no. 2, p. 321-361.

Min, K. D., 1975, Analytical and petrofabric studies of experimental faulted drape-folds in layered rock specimens, Ph.D. Dissertation, Dept. of Geophysics, Texas A&M University, 90 p.

Noble, J. P. A. and Ferguson, R. D., 1973, Facies relations at edge of Early Mid-Devonian carbonate shelf, South Nahonni River area, N. W. T., in Arctic Geology, Max G. Pitcher, ed., Am. Assoc. Pet. Geol. Mem. 19, p. 83-98.

Norris, D. K., 1973, Tectonic styles of northern Yukon Territory and northwestern District of Mackenzie, in Arctic geology, Max G. Pitcher, ed., Am. Assoc. Pet. Geol. Mem. 19, p. 23-40.

Obert, L. and Duvall, W. I., 1967, Rock mechanics and the design of structures in rock, John Wiley and Sons, Inc., New York.

Serata, S., Sukurai, S. and Adachi, T., 1972, Theory of aggregate rock behavior based on absolute three dimensional testing of rock salt, in Basic and Applied Rock Mechanics, K. E. Gray, ed., Proc. Tenth Symposium on Rock Mechanics, p. 431-473.

Teufel, L. W., 1975, Strain analysis of twinned calcites for two experimentally superposed deformations of Indiana Limestone, Geol. Soc. Am., Abstracts with Programs, v. 7, no. 2, p. 240.

Timoshenko, S. and Goodier, J. N., 1970, Theory of Elasticity, 3rd ed., McGraw-Hill, New York.

VITA

Lawrence Dana Dyke was born in Newmarket, Ontario, Canada on May 2, 1947. He is the son of Sidney L. Dyke and Imogene L. Dyke. He attended the University of British Columbia where he received a Bachelor of Science degree in geology in 1972. He has worked as a graduate assistant and project leader for the Geological Survey of Canada for six summers and as a field assistant for Noranda Exploration Co. Ltd. for two summers.

Permanent address: 5555 Greenleaf Road
West Vancouver, B.C., Canada

The typists for this thesis were Mrs. Linda Peoples and Mrs. Robin Leinhart.